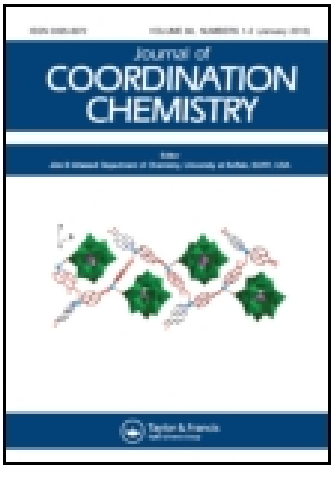

Journal of Coordination Chemistry
Publication details, including instructions for authors and subscription information:
http://www.tandfonline.com/loi/gcoo20

Two new 2-D frameworks based on tetra-copper(II)-substituted sandwich-type polyoxotungstate anions and $[Cu_2(dien)_2(OH)]^{3+}$ cations

Pengtao Ma[a], Yongna Zhang[a] & Jie Li[a]
[a] Key Laboratory of Polyoxometalate Chemistry of Henan Province, School of Chemistry and Chemical Engineering, Institute of Molecular and Crystal Engineering, Henan University, Kaifeng, China

Accepted author version posted online: 01 Jul 2014.Published online: 21 Jul 2014.

Journal of Coordination Chemistry, 2014
Vol. 67, No. 13, 2238–2248, http://dx.doi.org/10.1080/00958972.2014.940336

Two new 2-D frameworks based on tetra-copper(II)-substituted sandwich-type polyoxotungstate anions and $[Cu_2(dien)_2(OH)]^{3+}$ cations

PENGTAO MA*, YONGNA ZHANG and JIE LI

Key Laboratory of Polyoxometalate Chemistry of Henan Province, School of Chemistry and Chemical Engineering, Institute of Molecular and Crystal Engineering, Henan University, Kaifeng, China

(*Received 8 March 2014; accepted 9 June 2014*)

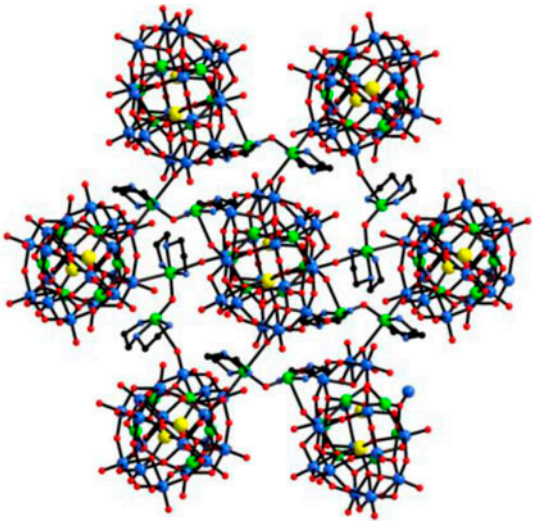

Two new organic–inorganic polyoxometalates with 2-D (6,3)-connected topology architecture $[Cu(dien)(H_2O)]_2\{[Cu_2(dien)_2(OH)]_2[Cu_4(B\text{-}\alpha\text{-}XW_9O_{33})_2]\}\cdot 4H_2O$ (X = Sb, **1;** X = As, **2**) (dien = diethylenetriamine) were hydrothermally synthesized.

Two new organic–inorganic polyoxometalates $[Cu(dien)(H_2O)]_2\{[Cu_2(dien)_2(OH)]_2[Cu_4(B\text{-}\alpha\text{-}XW_9O_{33})_2]\}\cdot 4H_2O$ (X = Sb, **1;** X = As, **2**) (dien = diethylenetriamine) were hydrothermally synthesized and characterized by elemental analysis, IR spectra, thermogravimetric (TG) analyses, and single-crystal X-ray diffraction. Both compounds are constructed from one four-coordinate $[Cu(dien)(H_2O)]^{2+}$, one $\{[Cu_2(dien)_2(OH)]_2[Cu_4(B\text{-}\alpha\text{-}XW_9O_{33})_2]\}$ building unit, and four water molecules of crystallization. Structural analysis shows that the sandwich-like polyoxotungstate

*Corresponding author. Email: mpt@henu.edu.cn

cluster anions $[Cu_4(B\text{-}\alpha\text{-}XW_9O_{33})_2]^{10-}$ are linked by six adjacent dimeric cations $[Cu_2(dien)_2(OH)]^{3+}$ into a 2-D architecture with a (6,3)-connected topology. Magnetic measurements of **1** and **2** exhibit the presence of antiferromagnetic interactions within the tetranuclear-Cu^{II} cluster.

Keywords: Polyoxometalate; Hydrothermal; Crystal structure; Sandwich-type

1. Introduction

Continuous interest in designing and making transition metal-substituted polyoxometalates (TMSPs) has persisted because of their impressive compositional diversity and versatile applications in catalysis, medicine, and materials science [1–3]. The progress of TMSP chemistry is principally driven by the synthesis and characterization of new compounds possessing unique topologies and performances. One of the effective approaches is to introduce interesting transition metal complexes (TMCs) acting as bridges or pendants into the framework of the inorganic POMs [4–6]. Hitherto, the classical Keggin fragments have often been used as the candidates mainly because the charge density of the surface oxygens can be increased either by reducing some of the metal centers or by replacing higher valence metal centers with lower valence metal centers [7–13]. However, composite materials constructed by trivacant Keggin fragments and TMC moieties remain less developed [14–18]. Within the class of TMSPs, sandwich-type polyoxometalates (POMs) represent the largest subclass [19–21], Sandwich-type POMs based on trivacant $[SbW_9O_{33}]^{9-}$ fragments are rarely reported and mostly pure inorganic [22–24], and organic–inorganic hybrid sandwich-type POMs built from $[SbW_9O_{33}]^{9-}$ fragments are undeveloped [25, 26].

Based on aforementioned considerations, we have focused on using various ligands in the reaction system of TM cations and lacunary polyoxotungstate anions in order to obtain new POM-based TM clusters functionalized by small organic molecules. In our synthetic strategy, diethylenetriamine (dien), a readily available ligand, seized our attention because compared to water it has stronger coordination ability to metal ions, consequently offering the possibility of substituting coordinated water molecules so as to influence the magnetic property of the copper center. Hydrothermal conditions shift a reaction from thermodynamic to kinetic control so that equilibrium phases are replaced by more structurally complicated metastable phases [27, 28]. Under hydrothermal environment, the reduced viscosity of the solvent enhances reaction reactivity of complicated metastable phases and further results in enhanced rates of solvent extraction of solids and crystal growth from solution. Since the different solubility problems can be minimized, a variety of organic and inorganic components can be introduced [28]. Fortunately, we have isolated two sandwich-type polyoxotungstates modified by dien ligands using hydrothermal methods, $[Cu(dien)(H_2O)]_2[Cu_2(dien)_2(OH)]_2[Cu_4(B\text{-}\alpha\text{-}XW_9O_{33})_2]\cdot 4H_2O$ (**1**) (X = Sb, **1**; X = As, **2**) (dien = diethylenetriamine), which differ from known examples built only by inorganic sandwich-type TMSPs. The common structural characteristic is that each $[Cu_4(B\text{-}\alpha\text{-}XW_9O_{33})_2]^{10-}$ (X = Sb for **1** and As for **2**) subunit links six adjacent complexes through six dimeric $[Cu_2(dien)_2(OH)]^{3+}$ bridges, forming a 2-D architecture with a (6,3)-connected topology. To the best of our knowledge, this kind of structure has been rarely reported.

2. Experimental

2.1. *Materials and physical measurements*

$(NH_4)_{18}[NaSb_9W_{21}O_{86}]\cdot 24H_2O$ was prepared according to the literature procedure [29] and identified by IR spectrum. All chemicals were of reagent grade and used without purification. Syntheses were carried out in 23 mL Teflon-lined autoclaves under autogenous pressure. The reaction vessels were filled to 50% volume capacity.

C, H, and N elemental analyses were performed on a Perkin-Elmer 240C elemental analyzer. Inductively coupled plasma (ICP) analysis was performed on a Perkin–Elmer Optima 2000 ICP-OES spectrometer. Infrared spectra were recorded on a Bruker VERTEX 70 IR spectrometer using KBr pellets from 400 to 4000 cm^{-1}. Thermogravimetric analyses were performed using a Perkin–Elmer7 thermal analyzer from 25 to 800 °C under a dry nitrogen atmosphere for **1** and **2** with a heating rate of 10 °C/min. XPS analyses for **1** were performed on an Axis Ultra (Kratos, UK) spectrometer with an Al Ka achromatic X-ray source. Variable temperature magnetic susceptibilities were carried out with a Quantum Design MPMS-5 magnetometer. Experimental susceptibilities were corrected for diamagnetism of the constituent atoms using Pascal's constants.

2.2. *Synthesis*

2.2.1. $[Cu(dien)(H_2O)]_2[Cu_2(dien)_2(OH)]_2[Cu_4(B\text{-}\alpha\text{-}SbW_9O_{33})_2]\cdot 4H_2O$ (1). A mixture of $(NH_4)_{18}[NaSb_9W_{21}O_{86}]\cdot 24H_2O$ (0.70 g, 0.1 mM), $CuCl_2\cdot 2H_2O$ (0.42 g, 2.5 mM), dien (0.05 mL), and H_2O (10 mL) was stirred for 1 h. The pH of the solution was adjusted to 5.4–6.0 with 2 M L^{-1} HCl. The mixture was transferred to a Teflon-lined stainless steel autoclave (23 mL). The Teflon-lined stainless steel autoclave was heated to 160 °C within 30 min and kept at 130 °C for five days, and then cooled to room temperature at a rate of 10 °C/h. Black–green block-like crystals of **1** were separated, washed with water and air-dried in a yield of 29% (based on Cu). Anal. Calcd for $C_{24}N_{18}H_{92}Cu_{10}O_{72}Sb_2W_{18}$ (5973.17): C, 4.83; H, 1.55; N, 4.22; Cu, 10.64; Sb, 4.08; W, 55.40. Found (%): C, 5.06; H, 1.49; N, 4.08; Cu, 10.36; Sb, 4.17; W, 55.92.

2.2.2. $[Cu(dien)(H_2O)]_2[Cu_2(dien)_2(OH)]_2[Cu_4(B\text{-}\alpha\text{-}AsW_9O_{33})_2]\cdot 4H_2O$ (2). A mixture of As_2O_3 (0.36 g, 1.8 mM), $Na_2WO_4\cdot 2H_2O$ (1.98 g, 6.0 mM), $CuCl_2\cdot 2H_2O$ (0.34 g, 2.0 mM), $Cu(CH_3COO)_2\cdot H_2O$ (0.40 g, 2.0 mM), phen·H_2O (0.20 g, 1.0 mM), dien (0.05 mL), and H_2O (10 mL) was stirred for 1 h. The pH of the solution was adjusted to 5.7–6.4 with 2 M L^{-1} HCl. The mixture was transferred to a Teflon-lined stainless steel autoclave (23 mL). The Teflon-lined stainless steel autoclave was kept at 160 °C for four days and then cooled to room temperature at a rate of 10 °C/h. Black–green rod-like crystals of **2** were separated, washed with water and air-dried in a yield of 27% (based on Cu). Anal. Calcd for $C_{24}N_{18}H_{92}Cu_{10}O_{72}As_2W_{18}$ (5879.49): C, 4.90; H, 1.57; N, 4.29; Cu, 10.81; As, 2.55; W, 56.28. Found (%): C, 5.12; H, 1.48; N, 4.11; Cu, 10.65; As, 2.64; W, 56.78.

2.3. *Crystallographic data collection and refinement*

A black–green crystal with dimensions 0.47 mm × 0.21 mm × 0.18 mm for **1** and 0.46 mm × 0.11 mm × 0.07 mm for **2** was stuck on a glass fiber and intensity data were collected at

296(2) K on a Bruker Smart Apex-II CCD diffractometer with graphite-monochromated Mo K_α radiation ($\lambda = 0.71073$ Å). Cell constants and an orientation matrix for data collection were obtained from least-squares refinements of the setting angles in the range of $1.85° \le \theta \le 25.00°$. Routine Lorentz polarization and an empirical absorption correction were applied to intensity data. On the basis of systematic absences and statistics of intensity, the space groups were *P2(1)/n*. Their structures were determined and the heavy atoms were found by direct methods using the SHELXTL-97 program package [30]. The remaining atoms were found from successive full-matrix least-squares refinements on F^2 and Fourier syntheses. No hydrogens associated with water molecules were located from the difference Fourier map. Positions of the hydrogens attached to carbon and nitrogen (except for bridging *N* of dien) were geometrically placed. All hydrogens were refined isotropically as a riding mode using the default SHELXTL parameters. For **1**, of 24,088 reflections, 8449 unique reflections ($R_{int} = 0.0579$) were considered observed [$I > 2\sigma(I)$]. For **2**, of 24,363 reflections, 8442 unique reflections ($R_{int} = 0.0393$) were considered observed [$I > 2\sigma(I)$]. Crystallographic data and structure refinements for **1** and **2** are summarized in table 1. Selected bond lengths for **1** and **2** are given in table 2.

3. Results and discussion

3.1. *Structural description*

Single-crystal structural analyses reveal that **1** and **2** are isostructural and crystallize in the same monoclinic space group *P2(1)/n*. Therefore, only the structure of **1** is described in detail. Their common structural feature is best described as a 2-D network constructed from

Table 1. Crystallographic data and structure refinement parameters for **1** and **2**.

Empirical formula	$C_{24}N_{18}H_{92}Cu_{10}O_{72}Sb_2W_{18}$ (**1**)	$C_{24}N_{18}H_{92}Cu_{10}O_{72}As_2W_{18}$ (**2**)
Molecular weight	5973.17	5879.49
Temperature (K)	296(2)	296(2)
Wavelength (Å)	0.71073	0.71073
Crystal system, space group	Monoclinic, *P2(1)/n*	Monoclinic, *P2(1)/n*
a (Å)	15.5924(16)	15.5488(15)
b (Å)	14.1241(14)	14.1218(13)
c (Å)	22.793(2)	22.769(2)
β (°)	106.156(2)	106.046(2)
V (Å^3)	4821.3(8)	4804.7(8)
Z	2	2
ρ_{Calcd} (g cm^{-3})	4.106	4.056
M (mm^{-1})	24.178	24.395
F (0 0 0)	5300	5228
Crystal size (mm)	0.47 × 0.21 × 0.18	0.46 × 0.11 × 0.07
θ Range for data collection (°)	1.85–25.00	1.85–25.00
Index range	$-18 \le h \le 18$, $-15 \le k \le 16$, $-27 \le l \le 26$	$-18 \le h \le 16$, $-16 \le k \le 14$, $-21 \le l \le 27$
Reflections collected/unique	24,088/8449 ($R_{int} = 0.0579$)	24,363/8442 ($R_{int} = 0.0393$)
Goodness-of-fit on F^2	1.041	1.045
Final *R* indices [$I > 2\sigma(I)$]	$R_1 = 0.0472$, $wR_2 = 0.1067$	$R_1 = 0.0290$, $wR_2 = 0.0682$
R indices (all data)	$R_1 = 0.0651$, $wR_2 = 0.1131$	$R_1 = 0.0376$, $wR_2 = 0.0708$

Table 2. Selected bond distances (Å) for **1** and **2**.

1		**2**	
Sb(1)–O(18)	1.962(10)	As(1)–O(18)	1.769(6)
Sb(1)–O(6)	1.967(10)	As(1)–O(6)	1.783(6)
Sb(1)–O(29)	1.970(11)	As(1)–O(29)	1.784(6)
Cu(1)–O(33)	1.948(14)	Cu(1)–O(33)	1.983(8)
Cu(1)–O(5)	1.989(14)	Cu(1)–O(5)	1.960(7)
Cu(1)–O(24)#1	1.997(12)	Cu(1)–O(24)#1	1.978(7)
Cu(1)–O(17)#1	2.082(14)	Cu(1)–O(17)#1	2.022(7)
Cu(2)–O(17)	1.978(14)	Cu(2)–O(17)	1.969(8)
Cu(2)–O(10)	1.985(13)	Cu(2)–O(10)	1.972(7)
Cu(2)–O(28)#1	1.986(15)	Cu(2)–O(28)#1	1.982(8)
Cu(2)–O(33)#1	2.044(14)	Cu(2)–O(33)#1	1.992(8)
Cu(3)–O(28)	1.917(14)	Cu(3)–O(28)	1.953(7)
Cu(3)–O(24)	2.021(13)	Cu(3)–O(24)	1.968(7)
Cu(3)–O(10)#1	2.028(15)	Cu(3)–O(10)#1	1.994(8)
Cu(3)–O(5)#1	2.032(14)	Cu(3)–O(5)#1	2.010(8)
Cu(4)–O(34)	1.953(12)	Cu(4)–O(34)	1.961(7)
Cu(4)–N(3)	1.997(15)	Cu(4)–N(1)	1.995(10)
Cu(4)–N(2)	2.016(14)	Cu(4)–N(3)	2.015(9)
Cu(4)–N(1)	2.039(16)	Cu(4)–N(2)	2.018(8)
Cu(5)–O(34)	1.942(12)	Cu(5)–O(34)	1.935(7)
Cu(5)–N(5)	1.983(16)	Cu(5)–N(6)	1.991(9)
Cu(5)–N(6)	2.009(17)	Cu(5)–N(5)	1.999(9)
Cu(5)–N(4)	2.017(17)	Cu(5)–N(4)	2.022(10)
Cu(6)–N(9)	1.990(24)	Cu(6)–N(7)	2.00(2)
Cu(6)–N(7)	1.996(34)	Cu(6)–N(9)	2.001(12)
Cu(6)—N(8)	2.010(21)	Cu(6)–N(8)	2.019(11)
Cu(6)–O(1W)	2.466(21)	Cu(6)–O(1W)	2.476(11)

Note: Symmetry codes: #1 $-x,-y+2,-z$.

$\{[Cu_2(dien)_2(OH)]_2[Cu_4(B\text{-}\alpha\text{-}XW_9O_{33})_2]\}$ (X = Sb for **1** and As for **2**) building units governed by the $[Cu_2(dien)_2(OH)]^{3+}$ functionality. The structural unit of **1** consists of a new polyoxoanion $\{[Cu_2(dien)_2(OH)]_2[Cu_4(B\text{-}\alpha\text{-}SbW_9O_{33})_2]\}^{4-}$, two four-coordinate copper complex cations $[Cu(dien)(H_2O)]^{2+}$, and four waters of crystallization. As shown in figure 1(a), the centrosymmetric polyoxoanion $\{[Cu_2(dien)_2(OH)]_2[Cu_4(B\text{-}\alpha\text{-}SbW_9O_{33})_2]\}^{4-}$ contains a tetra-Cu^{II}-sandwiched $[Cu_4(B\text{-}\alpha\text{-}SbW_9O_{33})_2]^{10-}$ core, on which four unique dimeric

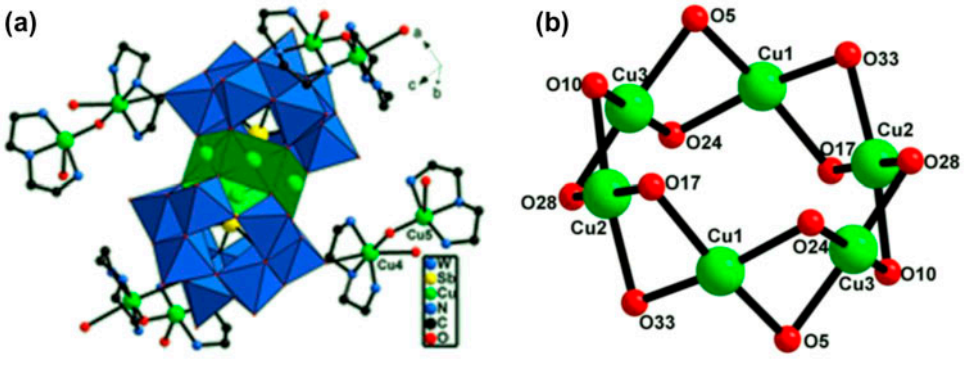

Figure 1. (a) Combined polyhedral/ball-and-stick view of the asymmetric sandwich-type polyoxoanion of **1**. (b) Ball-and-stick view of the tetra-Cu cluster $\{Cu_4O_{12}\}$.

coordination cations $[Cu_2(dien)_2(OH)]^{3+}$ serve as bridges connecting adjacent sandwiched subunits $[Cu_4(B\text{-}\alpha\text{-}SbW_9O_{33})_2]^{10-}$ forming a 2-D layer. Alternatively, this subunit can also be viewed as a combination of two half-units $\{[Cu_2(dien)_2(OH)]_2[Cu_2(B\text{-}\alpha\text{-}SbW_9O_{33})]\}$ related by an inversion center (0,1,0). The bond valence sum (BVS) [31] value for O(34) in **1** is significantly lower (0.96, near to 1), suggesting the probable monoprotonated position.

The tetra-Cu^{II}-sandwiched $[Cu_4(B\text{-}\alpha\text{-}SbW_9O_{33})_2]\}^{6-}$ fragment in **1** is distinct from the reported classical tetra-nuclear TM-sandwiched POM, such as $[B\text{-}\beta\text{-}Fe^{III}_4(H_2O)_8(SbW_9O_{33})_2]^{6-}$ polyoxoanion [32]. Obviously, four disordered copper ions in **1** [as shown in figure 1(a) and (b)] locate on six positions with an occupancy of 2/3 for Cu, forming a centrosymmetric six-membered cycle with an interior angle sum of 720° as a plane hexagon. And each Cu position in **1** is coordinated by four oxygens from two different $[SbW_9O_{33}]^{9-}$ moieties, however, four Fe ions in $[B\text{-}\beta\text{-}Fe^{III}_4(H_2O)_8(SbW_9O_{33})_2]^{6-}$ are linked by six oxygens from three different $[SbW_9O_{33}]^{9-}$ moieties. The arrangement of hexagonal $\{Cu_4\}$ clusters in the belt region is sandwiched by two $[B\text{-}\alpha\text{-}SbW_9O_{33}]^{9-}$ moieties via exposed 12 bridging oxygens from lacunae of two $[B\text{-}\alpha\text{-}SbW_9O_{33}]^{9-}$ units (12 μ_3-O from 12 WO_6 groups). In addition, the coordination in **1** is different from the coplanar-shaped hexa-Cu^{II}-sandwiched arsenotungstate reported by us [21].

In the structural unit of **1**, there are six crystallographically unique Cu^{2+} cations. The copper ions of Cu(1), Cu(2), and Cu(3) are sandwiched by two $[SbW_9O_{33}]^{9-}$ subunits and fused together with their symmetrical atoms forming a rhombic $\{Cu_4\}$ cluster by edge-sharing, which display a quadrangle geometry, whose plane is furnished by the oxygens from four WO_6 groups of two different $[SbW_9O_{33}]^{9-}$ ligands with Cu–O bond lengths of 1.917(14)–2.082(14) Å. Cu(4) and Cu(5) are joined together by a OH^- forming a dimeric coordination cation $[Cu_2(dien)_2(OH)]^{3+}$, grafted on the polyoxoanion skeleton via one or two bridging oxygens. Differently, Cu4 is connected with two polyoxoanion units, whereas, Cu5 is only grafted on another polyoxoanion skeleton [figure 2(a)]. Therefore, Cu(4) displays a distorted octahedral geometry, in which three nitrogens from one dien [Cu(4)–N: 1.997(15)–2.039(12) Å] and one hydroxyl oxygen [Cu(4)–O_{OH}: 1.953(12) Å] build the basal plane and two bridging oxygens from the POM backbone [Cu(4)–O_{POM}: 2.721(13)

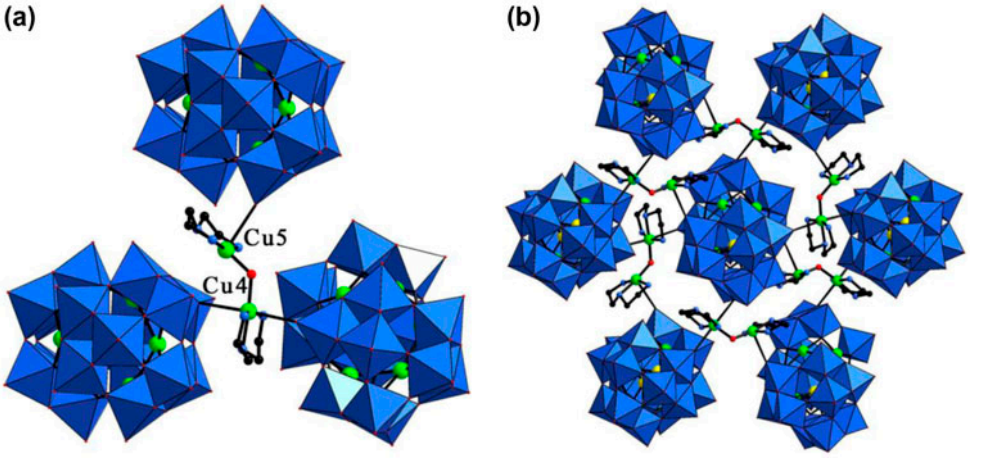

Figure 2. Connections of (a) the dimeric cation $[Cu_2(dien)_2(OH)]^{3+}$ bridge and (b) polyoxoanion $[Cu_4(B\text{-}\alpha\text{-}SbW_9O_{33})_2]^{10-}$ unit in **1**.

and 2.710(11) Å] occupy the two axial positions. Cu(5) resides in distorted tetragonal pyramidal geometry, coordinated by three nitrogens from one dien [Cu(5)–N: 1.983(16)–2.017 (17) Å] and one hydroxyl oxygen [Cu(5)–O_{OH}: 1.941(12) Å] forming the basal plane and one bridging oxygen from the POM backbone [Cu(5)–O_{POM}: 2.832(13) Å] sitting on the axial position. Additionally, Cu(6) complex cation is a discrete counter-cation displaying a seriously distorted tetrahedral environment, defined by three nitrogens from one dien [Cu(6)–N: 1.990(24)–2.010(21) Å] and one terminal water [Cu(6)–O_W: 2.466(21) Å]. The distance of two heteroatoms Sb···Sb is 4.919(2) Å in **1**, shorter than that in **2** (d(As···As) = 5.351(2) Å). The major reason is that the radius of Sb atom is bigger than that of As.

The structural feature of **1** is best described as a 2-D layer-like framework constructed from $\{[Cu_2(dien)_2(OH)]_2[Cu_4(B\text{-}\alpha\text{-}SbW_9O_{33})_2]\}$ building units. This kind of structure construction is mainly governed by the $[Cu_2(dien)_2(OH)]^{3+}$ functionality. Every dimeric cation linker $[Cu_2(dien)_2(OH)]^{3+}$ joins with three $[Cu_4(B\text{-}\alpha\text{-}SbW_9O_{33})_2]^{10-}$ units, synchronously, every $[Cu_4(B\text{-}\alpha\text{-}SbW_9O_{33})_2]^{10-}$ links with six adjacent same ones through six dimeric $[Cu_2(dien)_2(OH)]^{3+}$ bridges [figure 2(b)]. With this connection fashion, a 2-D layer-like architecture with (6,3)-2-D topology along the *bc* plane (figure 3) is formed, which obviously differs from these known examples only containing inorganic sandwich-type TMSPs [22–24]. Two 2-D trivacant Keggin POTs $CsNa_2[\{Sn(CH_3)_2\}_3(H_2O)_4(\beta\text{-}XW_9O_{33})]\cdot 7H_2O$ ($X = As^{III}/Sb^{III}$) were made by the conventional aqueous solution method [33] and a 2-D tetra-TM-sandwiched POT reported by Guoyu Yang under hydrothermal conditions [34]. To the best of our knowledge, **1** and **2** represent the rare (6,3)-2-D topological network in sandwich-type POM chemistry.

3.2. *IR spectra*

IR spectra of **1** and **2** display characteristic vibration patterns derived from the trivacant Keggin framework (figure 4) at 700–1000 cm^{-1}. Four characteristic bands at 937, 723, 889, and 758 cm^{-1} for **1**, and at 941, 730, 869, and 770 cm^{-1} for **2** are attributed to stretching vibration of $\nu(W\text{–}O_t)$, $\nu(X\text{–}O_a)$ (X = Sb/As), $\nu(W\text{–}O_b)$, and $\nu(W\text{–}O_c)$, respectively [35]. In

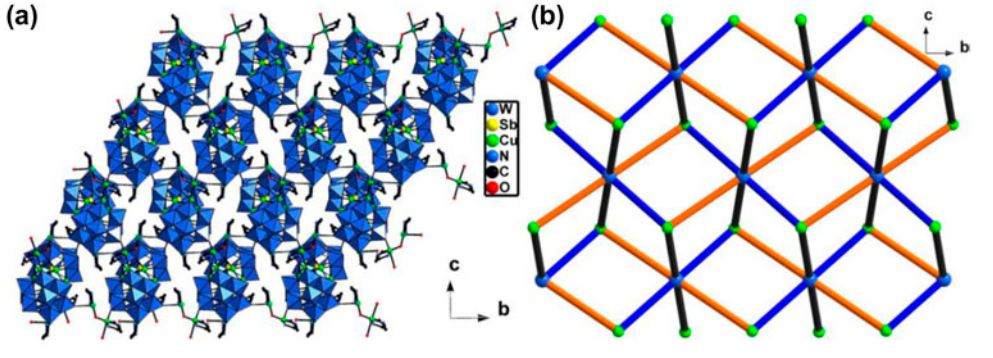

Figure 3. (a) Combined polyhedral/ball-and-stick and (b) topology structure of the two-dimensional layer-like arrangement of **1** viewed down the *a* axis, which is built from $[Cu_4(B\text{-}\alpha\text{-}SbW_9O_{33})_2]^{10-}$ polyoxoanions via $[Cu_2(dien)_2(OH)]^{3+}$ bridges. The blue nodes represent $[Cu_4(B\text{-}\alpha\text{-}SbW_9O_{33})_2]^{10-}$ building units; the green nodes represent $[Cu_2(dien)_2(OH)]^{3+}$ linkers; the light orange, black, and blue rods represent three different {Cu(dien)} bridges [see figure 3(a)], respectively. Some discrete fragments ions and solvent molecules were omitted for clarity (see http://dx.doi.org/10.1080/00958972.2014.940336 for color version).

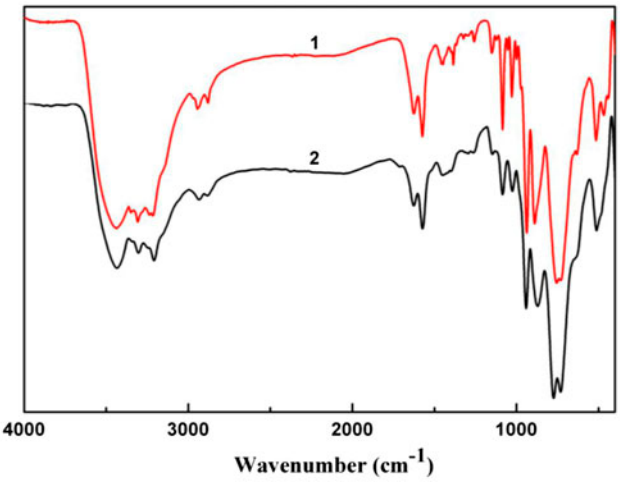

Figure 4. IR spectra of 1 and 2.

addition, stretches of –OH, $–NH_2$, and $–CH_2$ are observed at 3441, 3305 and 3214, 2941 and 2879 cm^{-1} for **1**, and at 3435, 3300 and 3208, 2930 and 2878 cm^{-1} for **2**, respectively. Bands at 1628, 1570, and 1452 cm^{-1} for **1**, and at 1630, 1571, and 1451 cm^{-1} for **2** are assigned to bending vibration of –OH, $–NH_2$, and $–CH_2$, respectively [36]. The vibration pattern of ν(C–N) is at 1383 cm^{-1} for **1** and 1395 cm^{-1} for **2**. The occurrence of these resonance signals confirms the presence of organic amine groups, which are consistent with the single-crystal structural analyses.

3.3. *XPS spectra*

The BVS calculations [37] suggest that all tungstens are of +6 oxidation state and Cu +2 oxidation state in **1**. The XPS spectra of **1** further confirm the calculated results. The XPS spectra (figure 5) of **1** in the energy regions of $W4f_{7/2}$ and $Cu2p_{3/2}$ show peaks at 34.4 and 933.7 eV, attributable to W^{6+} and Cu^{2+}, respectively. These results are consistent with the

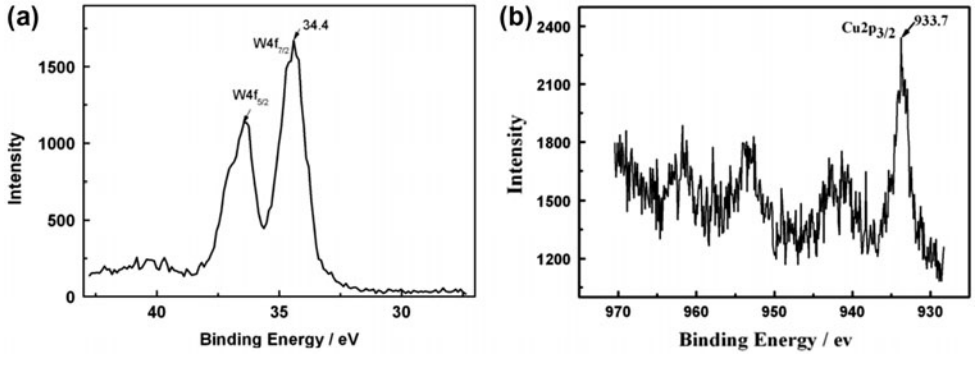

Figure 5. The XPS spectra of **1**.

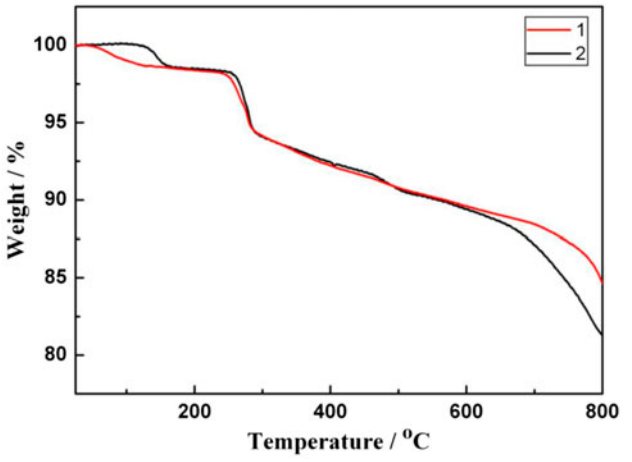

Figure 6. The TG curves of **1** and **2**.

binding energy values of W_{4f} in α-$SiW_{12}O_{40}$ [38] and Cu_{2p} in CuO [39], which are 35.3 and 934.1 eV, respectively. All these results confirm the valences of W and Cu.

3.4. *Thermogravimatric analysis*

In order to estimate the lattice-water content and the thermal stability of **1** and **2**, TG analyses were carried out from 25 to 800 °C (figure 6). The TG curves of **1** and **2** show two similar steps of weight losses. The first weight loss of 1.32% (Calcd 1.21%) for **1** is from 25 to 155 and 1.37% (Calcd 1.22%) for **2** from 25 to 145 °C, assigned to release of four lattice waters. The second stage of losing weight of 10.45% (Calcd 11.12%) between 156 and 678 °C for **1** and 10.87% (Calcd 11.29%) between 146 and 760 °C for **2** correspond to the loss of two coordinated water molecules, two OH^-, and six dien molecules.

3.5. *Magnetic properties*

The temperature dependence of the magnetic susceptibility of **1** and **2** under an applied field of 1 kOe is shown in figure 7 in the form of χ_m, $\chi_m T$, χ_m^{-1} *versus* T plots. For **1**, χ_m slowly increases from 0.013 emu M^{-1} at 300 K to 0.069 emu M^{-1} at 32 K, then exponentially to a maximum of 0.923 emu M^{-1} at 2 K. Comparison of the 300 K $\chi_m T$ value (3.85 emu K M^{-1}) at room temperature to that of 3.75 emu K M^{-1} for 10 non-interacting Cu(II) ($S = 1/2$) ions with $g = 2.0$ indicates that no spin exchange interactions exist between the Cu^{2+} centers and an $ST = 0$ ground state. Upon cooling, the $\chi_m T$ value increases gradually until 98 K; subsequently, slowly decreasing until 12 K, then radically decreasing to the minimum value 1.84 emu K M^{-1} at 2 K. Similar to **1**, the χ_m value of **2** slowly increases from 0.013 emu M^{-1} at 300 K to 0.094 emu M^{-1} at 32 K, then exponentially to a maximum of 1.240 emu M^{-1} at 2 K. Accordingly, the $\chi_m T$ value 3.77 emu K M^{-1} for **2** at room temperature almost equals to the 10 non-interacting Cu(II) ($S = 1/2$, $g = 2.0$) ions (3.75 emu K M^{-1}). As the temperature is lowered, the $\chi_m T$ value decreases steadily until 78 K, followed by a slow decrease at lower temperatures. Below 12 K, the $\chi_m T$ value sharply drops to a minimum value

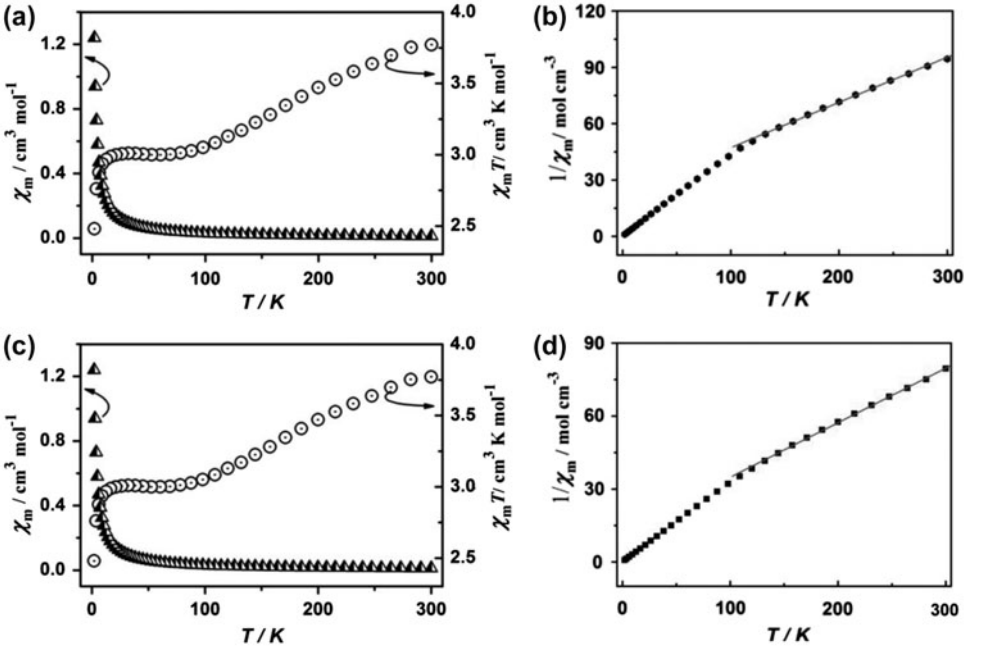

Figure 7. (a) $\chi_m T$ and χ_m as a function of temperature T for **1**. (b) $\chi_m T$ and χ_m *vs.* T for **2**. (c) χ_m^{-1} *vs.* T from 120 to 300 K for **1**. (d) χ_m^{-1} *vs.* T from 120 to 300 K for **2**. The red solid lines represent the fit to experimental data.

2.48 emu K M^{-1} at 2 K, indicating the presence of weak antiferromagnetic coupling. Furthermore, the magnetic susceptibility data between 120 and 300 K follow the Curie–Weiss equation $\chi_m = C/(T-\theta)$ with $C = 0.081$ emu K M^{-1} and $\theta = -0.018$ K for **1** and $C = 0.043$ emu K M^{-1} and $\theta = -0.104$ K for **2** [figure 7(c) and (d)]. These behaviors indicate the presence of the weak antiferromagnetic exchange interactions within the $\{Cu_4\}$ cluster in both compounds.

4. Conclusion

We have hydrothermally synthesized two new organic–inorganic hybrid polyoxotungstates based on $[Cu_4(B\text{-}\alpha\text{-}XW_9O_{33})_2]^{10-}$ (X = Sb or As) units, which will enrich significantly the field of sandwich-type polyoxotungstates, and will promote further development of chemistry of polyoxometalates. Moreover, the successful preparation of organic–inorganic hybrid materials will provide a feasible and effective synthetic route for searching and exploring organic–inorganic hybrids based on polyoxometalates as a basic framework in synthetic chemistry and material science.

Supplementary material

Crystallographic data for the structural analysis have been deposited with the Cambridge Crystallographic Data Center, CCDC reference number 978225 for **1** and 989240 for **2**. These data can obtained free of charge via http://www.ccdc.cam.ac.uk/data_request/cif or from the Cambridge Crystallographic Data Center, 12 Union Road, Cambridge CB2 1EZ, UK (Fax: +44 1223 336033; E-mail: deposit@ccdc.cam.ac.uk).

Funding

We are grateful to the financial support by the International Technology Cooperation Project of Science and Technology Department of Henan Province of China [grant number 124300510050] and the Foundation of Education Department of Henan Province [grant number 12A150004], [grant number 14A150028].

References

[1] M.T. Pope. *Heteropoly and Isopoly Oxometalates*, Springer-Verlag, Berlin (1983).
[2] E. Coronado, C. Giménez-Saiz, C.J. Gómez-García. *Coord. Chem. Rev.*, **249**, 1776 (2005).
[3] T. Akutagawa, D. Endo, S.I. Noro, L. Cronin, T. Nakamura. *Coord. Chem. Rev.*, **251**, 2547 (2007).
[4] P. Gouzerh, A. Proust. *Chem. Rev.*, **98**, 77 (1998).
[5] B. Liu, L. Li, Y. Zhang, Y. Ma, H. Hu, G. Xue. *Inorg. Chem.*, **50**, 9172 (2011).
[6] E. Antonova, C. Näther, P. Kögerler, W. Bensch. *Inorg. Chem.*, **51**, 2318 (2012).
[7] V.S. Shivaiah, S.K. Das. *Inorg. Chem.*, **44**, 8846 (2005).
[8] A. Müller, W. Plass, E. Krickemeyer, S. Dillinger, H. Bögge, A. Armatage, A. Proust, C. Beugholt, U. Bergmann. *Angew. Chem. Int. Ed. Engl.*, **33**, 849 (1994).
[9] M. Yuan, Y. Li, E. Wang, C. Tian, L. Wang, C. Hu, N. Hu. *Inorg. Chem.*, **42**, 3670 (2003).
[10] Y. Xu, K.-L. Zhang, Y. Zhang, X.-Z. You, J.-Q. Xu. *Chem. Commun.*, 153 (2000).
[11] F.X. Liu, C. Marchal-Roch, P. Bouchard, J. Marrot, J.P. Simonato, G. Hervé, F. Sécheresse. *Inorg. Chem.*, **43**, 2240 (2004).
[12] S. Reinoso, P. Vitoria, J.M. Gutiérrez-Zorrilla, L. Lezama, L. San Felices, J.I. Beitia. *Inorg. Chem.*, **44**, 9731 (2005).
[13] Y. Lu, Y. Xu, E. Wang, J. Lü, C. Hu, L. Xu. *Cryst. Growth Des.*, **5**, 257 (2005).
[14] C.M. Wang, S.T. Zheng, G.Y. Yang. *Inorg. Chem.*, **46**, 616 (2007).
[15] N. Belai, M.T. Pope. *Chem. Commun.*, 5760 (2005).
[16] U. Kortz, F. Hussain, M. Reicke. *Angew. Chem. Int. Ed.*, **44**, 3773 (2005).
[17] S.T. Zheng, D.Q. Yuan, H.P. Jia, J. Zhang, G.Y. Yang. *Chem. Commun.*, 1858 (2007).
[18] H. Liu, C. Qin, Y.G. Wei, L. Xu, G.G. Gao, F.Y. Li, X.S. Qu. *Inorg. Chem.*, **47**, 4166 (2008).
[19] Y.H. Fan, M.M. Li, D.B. Dang, Y. Bai, X.Z. Li, Y.P. Zhao, J.Y. Niu. *J. Coord. Chem.*, **66**, 946 (2013).
[20] L. Yang, J. Zhao, J.W. Zhao, J.Y. Niu. *J. Coord. Chem.*, **65**, 3363 (2012).
[21] J.A. Hua, S.Z. Li, X. Ma, P.T. Ma, J.P. Wang, J.Y. Niu. *J. Coord. Chem.*, **65**, 1740 (2012).
[22] Q. Shan, K. Yu, C.X. Wang, Z.H. Su, J. Gu, B.B. Zhou. *J. Coord. Chem.*, **66**, 402 (2013).
[23] Z.S. Wang, Z.M. Zhang, Y.G. Li, X.B. Han, H. Duan, E.B. Wang. *J. Coord. Chem.*, **65**, 1443 (2012).
[24] Y.H. Liu, P.T. Ma, J.P. Wang. *J. Coord. Chem.*, **61**, 936 (2008).
[25] C. Zhao, C.S. Kambara, Y. Yang, A.L. Kaledin, D.G. Musaev, T. Lian, C.L. Hill. *Inorg. Chem.*, **52**, 671 (2013).
[26] J.P. Wang, P.T. Ma, J. Li, H.Y. Niu, J.Y. Niu. *Chem. Asian J.*, **3**, 822 (2008).
[27] J. Gopalakrishnan. *Chem. Mater.*, **7**, 1265 (1995).
[28] H. Jin, Y. Qi, E. Wang, Y. Li, C. Qin, X. Wang, S. Chang. *Eur. J. Inorg. Chem.*, 4541, (2006).
[29] G. Herva, A. Taza. *Inorg. Synth.*, **27**, 120 (1990).
[30] G.M. Sheldrick. *SHELXTL 97*, University of Göttingen, Göttingen (1997).
[31] I.D. Brown, D. Altermatt. *Acta Crystallogr., Sect. B*, **41**, 244 (1985).
[32] A. Dolbecq, J.D. Compain, P. Mialane, J. Marrot, E. Rivière, F. Sécheresse. *Inorg. Chem.*, **47**, 3371 (2008).
[33] F. Hussain, M. Reicke, U. Kortz. *Eur. J. Inorg. Chem.*, 2733 (2004).
[34] J.W. Zhao, B. Li, S.T. Zheng, G.Y. Yang. *Cryst. Growth Des.*, **7**, 2658 (2007).
[35] J.W. Zhao, J. Zhang, S.T. Zheng, G.Y. Yang. *J. Struct. Chem.*, **27**, 933 (2008).
[36] Y.B. Liu, X.B. Cui, J.Q. Xu, Y.K. Lu, J. Liu, Q.B. Zhang, T.G. Wang. *J. Mol. Struct.*, **825**, 45 (2006).
[37] I.D. Brownand, D. Altermatt. *Acta Cryst.*, **41**, 244 (1985).
[38] Y.H. Feng, Z.G. Han, J. Peng, J. Lu, B. Xue, L. Li, H.Y. Ma, E.B. Wang. *Mater. Lett.*, **60**, 1588 (2006).
[39] V.I. Nefedov, M.N. Firsov, I.S. Shaplygin. *J. Electron Spectrosc. Relat. Phenom.*, **26**, 65 (1982).